Journal of Nuclear Materials 385 (2009) 538–544

Contents lists available at ScienceDirect

Journal of Nuclear Materials

journal homepage: www.elsevier.com/locate/jnucmat

Gaseous hydrogen embrittlement of PH 13-8 Mo steel

Y.S. Ding [a], L.W. Tsay [a,*], M.F. Chiang [b,1], C. Chen [b,1]

[a] Institute of Materials Engineering, National Taiwan Ocean University, Keelung 202, Taiwan, ROC
[b] Department of Materials Science and Engineering, National Taiwan University, Taipei 106, Taiwan, ROC

ARTICLE INFO

Article history:
Received 1 February 2008
Accepted 17 December 2008

ABSTRACT

In this study, notched tensile and fatigue crack growth tests in gaseous hydrogen were performed on PH 13-8 Mo stainless steel specimens at room temperature. These specimens were susceptible to hydrogen embrittlement (HE), but at different degrees, depending on the aging conditions or the microstructures of the alloys. In hydrogen, the accelerated fatigue crack growth rate (FCGR) usually accompanied a reduced notched tensile strength (NTS) of the specimens, i.e., the faster the FCGR the lower the NTS. It was proposed that the same fracture mechanism could be applied to these two different types of specimens, regardless of the loading conditions. Rapid fatigue crack growth and high NTS loss were found in the H800 (426 °C under-aged) and H900 (482 °C peak-aged) specimens. The HE susceptibility of the steel was reduced by increasing the aging temperature above 593 °C, which was attributed to the increased amount of austenite in the structure. Extensive quasi-cleavage fracture was observed for the specimens that were deteriorated severely by HE.

1. Introduction

PH 13-8 Mo, a precipitation-hardening martensitic stainless steel (SS), is often used as a structural material for critical applications where a combination of high strength and good corrosion resistance is essential. With aging in the temperature range of 450–620 °C, the alloy achieves a high strength by the uniform precipitation of fine NiAl precipitates in irregular blocky units of lath martensite [1,2]. The fine NiAl precipitates are found to resist coarsening and maintain coherency with the matrix even when over-aged at 620 °C for 4 h [1,3]. The segregation of Mo and Cr to the precipitate/matrix interfaces is suggested to suppress the coarsening of the NiAl precipitates [1]. Meanwhile, the reverted austenite islands formed mainly at the lath boundaries lead to an obvious drop in strength/hardness [3]. The strength and hardness decrease, while the ductility and toughness increase, as the aging temperature is raised in the cast PH 13-8 Mo steel [4,5].

The severity of hydrogen embrittlement (HE) in high strength steels is known to be influenced by several factors such as hydrogen concentration, microstructures, strength level, stress state, grain size and cold work, etc. As with all high strength steels, HE affects the mechanical properties and fracture behavior of PH 13-8 Mo steel [6–9], and the HE susceptibility decreases with increasing aging temperature [7,10]. Sulfide stress corrosion cracking is a manifestation of hydrogen embrittlement [11,12] and provides a much severe condition as compared to cracking in gaseous hydrogen [13]. When aged at or above 620 °C, the resistance of the steel to sulfide stress corrosion cracking is substantially improved, due to the formation of considerable amounts of rather stable austenite in the structure [7]. A comparison of steels of the same strength level reveals that the resistance to sulfide stress cracking is generally in the descending order of PH 13-8, PH 17-4, PH 15-5, and 410 SS [14]. This could be attributed to the greater amount of austenite in the PH 13-8 Mo steel as compared to others.

The effect of hydrogen on crack growth that depends on the loading status can be divided into two categories: static loading or cyclic loading. A slow extension rate tensile test is often utilized to determine the deteriorated tensile properties of an alloy in hydrogen-containing environments [12,15]. As a result, this test can be applied to evaluate the relative HE susceptibility of different alloys. For engineering applications, a high strength alloy may encounter the problem of hydrogen-accelerated fatigue crack growth in service. In the published literature, very few studies have been carried out to evaluate the influence of hydrogen on deteriorating the mechanical properties of PH 13-8 Mo steel. The purpose of this investigation was to evaluate the hydrogen-accelerated fatigue crack growth of aged PH 13-8 Mo specimens and to correlate this with their NTS losses in gaseous hydrogen. The fracture appearances of various specimens were examined by scanning electron microscopy (SEM). A reduced HE susceptibility was also related to the beneficial microstructures and the strength level of the respective specimens.

2. Materials and experimental procedures

The chemical composition (in weight percent) of the PH 13-8 Mo steel used in this investigation was 12.65 Cr, 8.57 Ni, 2.20

* Corresponding author. Fax: +886 2 24625324.
E-mail address: b0186@mail.ntou.edu.tw (L.W. Tsay).
[1] Fax: +886 2 23634562.

0022-3115/$ - see front matter © 2008 Elsevier B.V. All rights reserved.
doi:10.1016/j.jnucmat.2008.12.048

Mo, 0.05 C, 0.07 Si, 0.05 Mn, 0.01 P, 0.004 S, 1.37 Al, and balance Fe. The alloy with a thickness of 4.1 mm was solution-treated (ST) in an inert environment at 930 °C (1700 F) for 40 min and then air-cooled to room temperature; the resultant specimen was designated as the ST specimen. The aging treatments were then performed at 427 °C (800 F), 482 °C (900 F), 538 °C (1000 F), 593 °C (1100 F) and 649 °C (1200 F) for 4 h, and the associated specimens were named as H800, H900, H1000, H1100 and H1200 specimens, respectively.

Ordinary tensile tests of smooth specimens with a gauge length of 25 mm were performed at room temperature in laboratory air under a strain rate of $6.67 \times 10^{-4}\ s^{-1}$, corresponding to a crosshead speed of 1 mm per minute. Notched tensile and fatigue crack growth tests were performed on distinct specimens at room temperature in air and gaseous hydrogen (0.2 MPa). The dimensions of the notched tensile and compact-tension (CT) specimens employed in this study are shown in Fig. 1. The double-edge notch specimen, which was made by an electrode-discharge wire cutter, had a notch angle of 60° and a notch radius of about 100 μm. The influence of HE on the NTS and the FCGR was evaluated by installing the specimen in a stainless steel chamber charging with gaseous hydrogen of 99.999% purity. Notched tensile tests were conducted at a slow extension rate of 1.5×10^{-3} mm/min, and the results were the average of at least three specimens for each testing condition. The HE susceptibility can be expressed as the reduction of NTS, or the NTS loss after hydrogen-charging, as follows:

$$\text{NTS loss } (\%) = \frac{\text{NTS (in air)} - \text{NTS (in H}_2\text{)}}{\text{NTS (in air)}}.$$

Fatigue crack growth tests were performed on the CT specimens in a computerized MTS system, with a loading frequency of 20 Hz and a constant amplitude of sinusoidal waveform at a stress ratio (R) of 0.1. The crack length was estimated on-line using a crack opening displacement gage mounted at the specimen edge. The compliance function provided by Saxena and Hudak [16] was used to determine the crack length which was checked by a 30× microscope. In the case of the specimens fatigued in hydrogen, the symbol 'H' was attached to the designated specimens.

An X-ray diffraction (XRD) method was employed to determine the amount of austenite in the specimens aged at different temperatures. The fracture appearances of assorted specimens were examined by a Hitachi S4100 scanning electron microscope (SEM) with the attention paid to the changes of fracture features. Thin foil specimens were prepared by a standard jet-polisher and then investigated with a 200 kV transmission electron microscope (TEM).

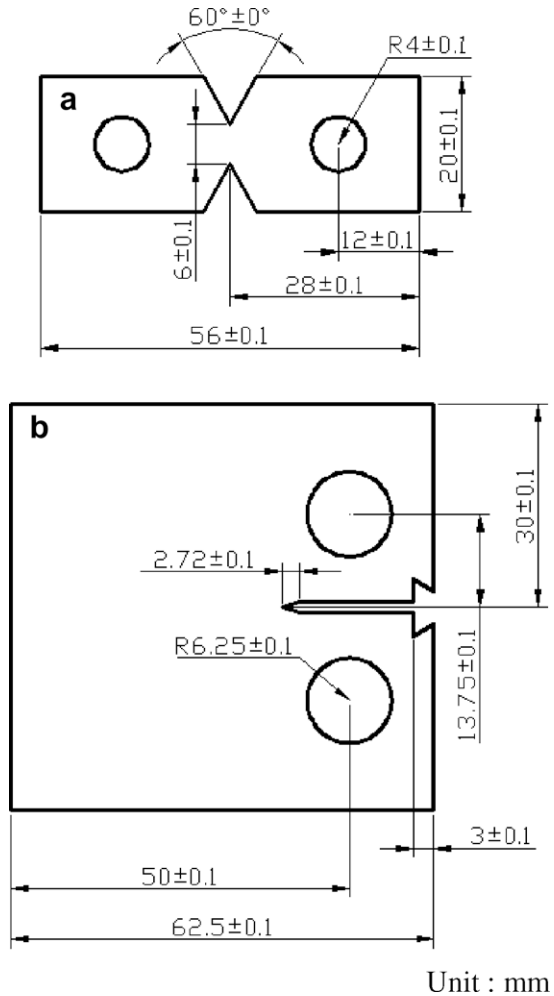

Fig. 1. Schematic diagrams showing the configuration of the (a) notched tensile specimens and (b) compact-tension (CT) specimens used in the experiment. Note that the thickness of both specimens is 4.0 mm.

3. Results

3.1. Hardness measurements and ordinary tensile test

Table 1 lists the hardness values and tensile properties of various specimens used in the study. The hardness of the H900 (H_{RC} 46) was higher than other specimens. Meanwhile, the H800 specimen (H_{RC} 38) was slightly harder than the H1100 (H_{RC} 36). For the over-aged specimen, e.g., the H1200 specimen, an obvious decrease in hardness to H_{RC} 28 was resulted which was even softer than the ST specimen (H_{RC} 31). The results indicated that the ultimate tensile strengths varied in the same manner as the hardnesses of the specimens, i.e., the higher the hardness, the greater the ultimate tensile strength. In contrast, the reverse is true for the ductility-hardness relationship, i.e., the higher the hardness the lower the ductility. Note that the H800 (yield strength or YS, 1020 MPa) and H1100 (YS, 985 MPa) specimens had the yield strength level around 1000 MPa, whereas the H1200 (YS, 708 MPa) and ST (YS, 650 MPa) specimens could be regarded as having roughly the same yield strength level. The H1200 specimen with a lower hardness but a higher yield strength than the ST specimen could be attributed to the presence of fine precipitates to impede dislocation motion more effectively during straining.

3.2. Microstructural observations

Fig. 2 contains TEM micrographs showing the microstructures of variously aged specimens. The ST specimen consisted of lath martensite with a high dislocation density and a small amount of

Table 1
Tensile properties of PH 13-8 Mo specimens heat-treated at various conditions.

Specimens	ST	H800	H900	H1000	H1100	H1200
UTS (MPa)[a]	1040	1225	1410	1360	1085	990
YS (MPa)[b]	650	1020	1305	1280	985	708
EL (%)[c]	15	13	11	11	17	21
Hardness (H_{RC})[d]	31	38	46	42	36	28

[a] Ultimate tensile strength.
[b] 0.2% offset yield strength.
[c] Elongation ($\Delta l/l$%).
[d] Rockwell hardness.

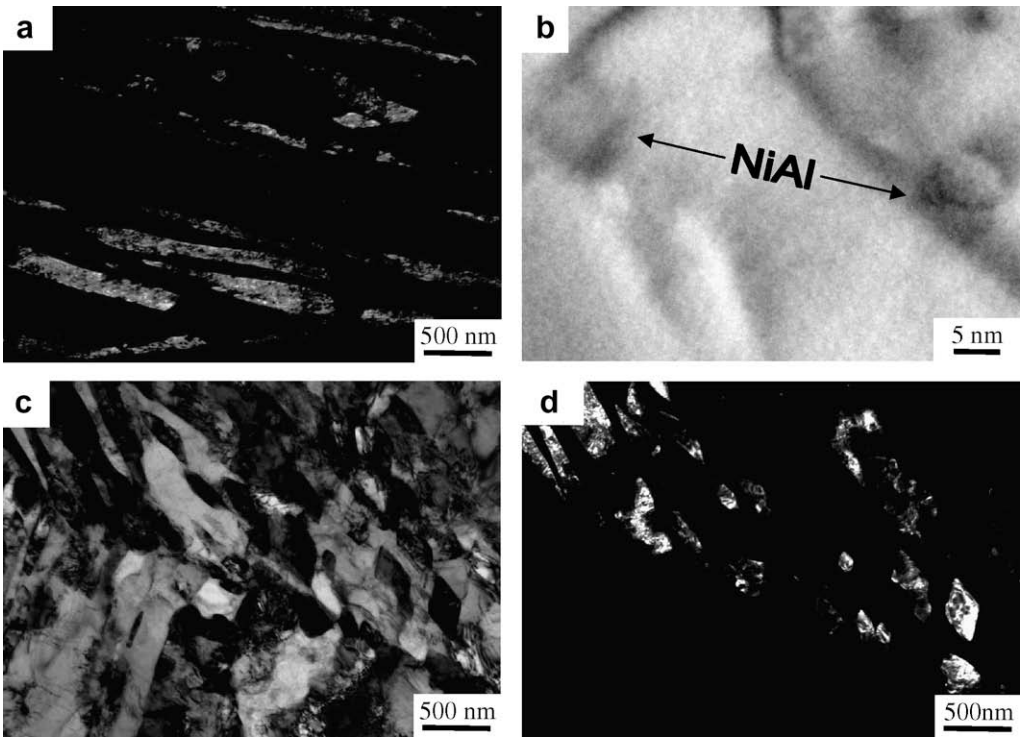

Fig. 2. TEM micrographs of the PH 13-8 Mo specimens: (a) dark field image of film-like austenite in the ST specimen; (b) ultra-fine NiAl precipitates in the H1000 specimen; (c) bright field and (d) dark field images showing island-like austenite in the H1100 specimen.

film-like retained austenite (Fig. 2(a)) at the lath boundaries. After aging the PH 13-8 Mo steel in the temperature range from 426 to 538 °C, ultra-fine NiAl particles (Fig. 2(b)) as well as a small amount of austenite film [1,3] were present mainly at the martensite lath boundaries. The XRD results indicated that the ST specimen contained very little retained austenite, less than 4%, which was the detecting limit of the instrument. It was noted that only a slight increase occurred in the austenite content for the specimens aged in the temperature range of 426–538 °C. In contrast, a significant increase in the austenite content was found for the specimens aged at higher temperatures, e.g., 12% for the H1100 and 17% for the H1200 specimens. Meanwhile, the change in the austenite morphology from film-like to island-like could be seen in the specimens aged at or above 593 °C (Fig. 2(c) and (d)). NiAl particles are reported to resist coarsening and maintain perfect coherency with the matrix even when over-aged at 620 °C for 4 h [1]. Therefore, the existence of a substantial amount of austenite was responsible for the remarkable decrease in the hardness of the over-aged specimens.

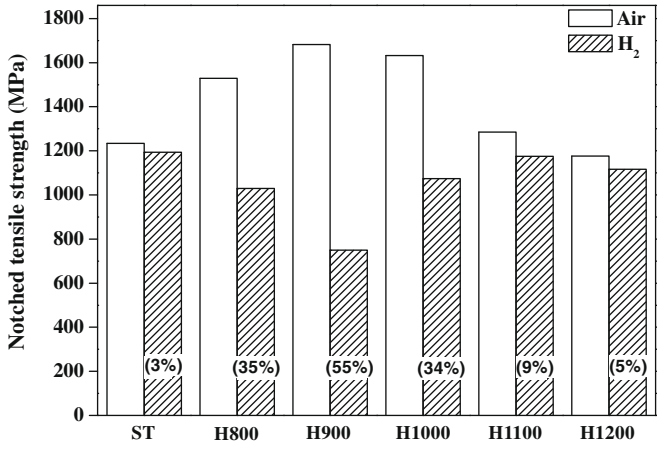

Fig. 3. The NTS values of PH 13-8 Mo specimens tested in air and hydrogen. Note that the percentages within parentheses indicate the NTS loss in hydrogen.

3.3. Notched tensile test

The NTS values of various specimens tested in air and gaseous hydrogen are given in Fig. 3. The NTS loss in hydrogen is often used as an index to assess the HE susceptibility of a given specimen. The H900 (peak-aged) specimen clearly had the highest NTS in air, while the H1200 had the lowest NTS among the specimens. Both ST and H1100 specimens had similar ultimate tensile strength in air and also possessed an equivalent NTS in air. The NTS of the H800 (under-aged) specimen was slightly lower than that of the H1000 (over-aged) in air. In general, the trend of variation in the NTS was in agreement with the specimen's ultimate tensile strength. In gaseous hydrogen, a deteriorated NTS was found for all specimens but at different degrees. The NTS losses were lower (more resistance to HE) for the ST, H1100 and H1200 specimens, in contrast to the higher NTS losses (more susceptible to HE) of the H800, H900 and H1000 specimens. Obviously, the specimens aged at or above 593 °C, e.g., the H1100 and H1200 specimens, showed a significant decrease in the HE susceptibility.

3.4. Fatigue crack growth test

The FCGR (da/dN) plotted against the stress intensity factor range (ΔK) for a variety of specimens is shown in Fig. 4. Fig. 4(a) reveals that the H800 and H900 specimens have similar fatigue crack growth behavior in air, whereas the H1200 specimen obviously exhibits a lower FCGR than the other specimens. For nearly the same level of yield strength (e.g., the ST and H1200, or the H800 and H1100 specimens), the over-aged (H1200 and H1100) specimens displayed lower FCGRs than the un-aged (ST) and

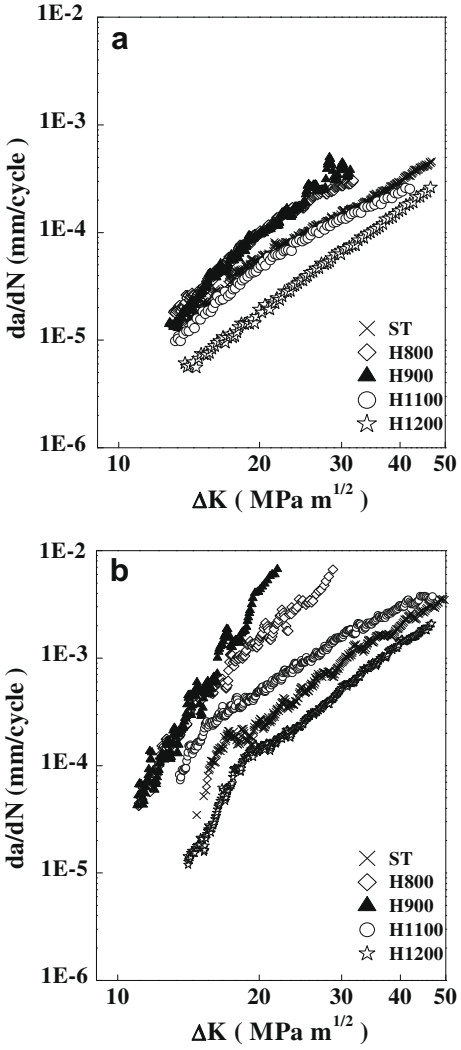

Fig. 4. Fatigue crack growth behaviors of PH 13-8 Mo specimens tested at room temperature in (a) laboratory air and (b) gaseous hydrogen.

under-aged (H800) specimens in air. In a previous study, a coarse austenite pool was found to be effective at impeding crack growth in the over-aged maraging steel weld [17]. It was deduced that the tough granular austenite in the over-aged specimens could resist the planar slip of dislocation, resulting in a reduced FCGR.

Fig. 4(b) shows da/dN vs. ΔK curves of the specimens fatigued in gaseous hydrogen, indicating the accelerated FCGRs of all specimens as compared with the counterpart specimens tested in air. It is evident that the hydrogen-accelerated crack growth was accompanied by a very high Paris-law gradient for the H800 and H900 specimens. These specimens had m values of about 3.75 in air and 5.48 in hydrogen, indicating that they were highly susceptible to hydrogen-accelerated fatigue crack growth. When aging at temperatures above 593 °C, the FCGRs in hydrogen decreased with an increase the aging temperature of the specimens. The H1200 specimen had the highest resistance to hydrogen-accelerated fatigue crack growth among the specimens tested. The difference in FCGRs between specimens with the same yield strength strongly suggests that the microstructures play an important role in affecting the fatigue crack growth behavior of the alloy in hydrogen. It is known that the trapping of hydrogen in the specimen, especially with beneficial strong traps such as austenite in the steel, can decrease hydrogen diffusivity [18,19] and delay the accumulation of hydrogen in the region ahead of the notch tip [19]. Thus, it was anticipated that the sensitivity to hydrogen-accelerated crack growth and hydrogen-induced cracking could be lower for the over-aged specimens.

3.5. Fractographic examinations

The macroscopic fracture appearances of some specimens after the fatigue and notched tensile tests are shown in Fig. 5. It is known that the presence of notches or cracks produces a triaxial stress state and is more likely to induce brittle fracture. The fatigue specimen with a sharp crack was expected to show a higher cracking susceptibility in hydrogen than the notched tensile specimen with a relatively dull notch tip. Fig. 5(a) and (b) is typical fatigue fracture appearances of the H1100 specimen tested in air and hydrogen, respectively. The results demonstrate that the change in testing environments seemed to have little influence on the macro-fracture morphology of the CT specimens. However, a lot of shiny spots decorating the fracture surface could be observed for the specimens tested in hydrogen. These shiny spots on the fracture surface were associated with the flat brittle fracture. In the case of the notched tensile tests, the specimens having low NTS losses in hydrogen exhibit large slant fracture regions accompanied with a noticeable thickness reduction as shown in Fig. 5(c). This implies that the occurrence of notch-blunting during plastic deformation helped to alleviate the effect of stress concentration, and therefore reduced the likelihood of HE. On the other hand, a significant change in the fracture appearance was found in the specimens with remarkable NTS losses in hydrogen, as shown in Fig. 5(d), in which an extensive region of flat fracture can be seen.

Fig. 6 contains SEM fractographs showing the tensile fracture appearance of the specimens aged at various temperatures. The fracture appearance of all smooth tensile specimens shows a predominantly ductile dimple fracture (Fig. 6(a)). For the H900 specimen, the fracture surface consists of a small amount of quasi-cleavage fracture mixed with fine dimples (Fig. 6(b)). In the case of the notched tensile specimens tested in hydrogen, the H800 and H900 specimens (Fig. 6(c) and (d)) display quasi-cleavage mixed with dimple fractures, but with more quasi-cleavage in the latter. The trend is that the specimens with lower HE susceptibilities exhibited more of the ductile dimple fracture on the fracture surfaces. HE or hydrogen-assisted fatigue crack growth would lead to an intergranular fracture mode of ultra-high strength steels in a more severe environment [20–23], however, it was not the case for PH 13-8 Mo steel in gaseous hydrogen; intergranular fracture of the specimens was not observed.

Typical fatigue fracture morphologies of several specimens tested in air or gaseous hydrogen are shown in Fig. 7. The fatigue fracture appearance of all specimens tested in air revealed a typically transgranular fatigue fracture (Fig. 7(a)). However, the fracture surface revealed the trace of lath martensite morphology (Fig. 7(b)) for the specimens aged at or above 593 °C. For the specimens tested in hydrogen, an extensive quasi-cleavage fracture (Fig. 7(c)) was observed, instead of the transgranular fatigue. The brittle fracture was evident for the specimens with increased FCGRs tested in hydrogen. It is important to note that a decline in the extent of quasi-cleavage in the H1200 specimen (Fig. 7(d)) demonstrated its improved resistance to hydrogen-accelerated fatigue crack growth. The extensive brittle fracture of PH 13-8 Mo steel was attributed to the deteriorating effect of HE, leading to increased FCGRs and NTS losses in hydrogen.

4. Discussion

The diffusion of hydrogen occurs not only down the concentration gradient but also toward the location of high hydrostatic

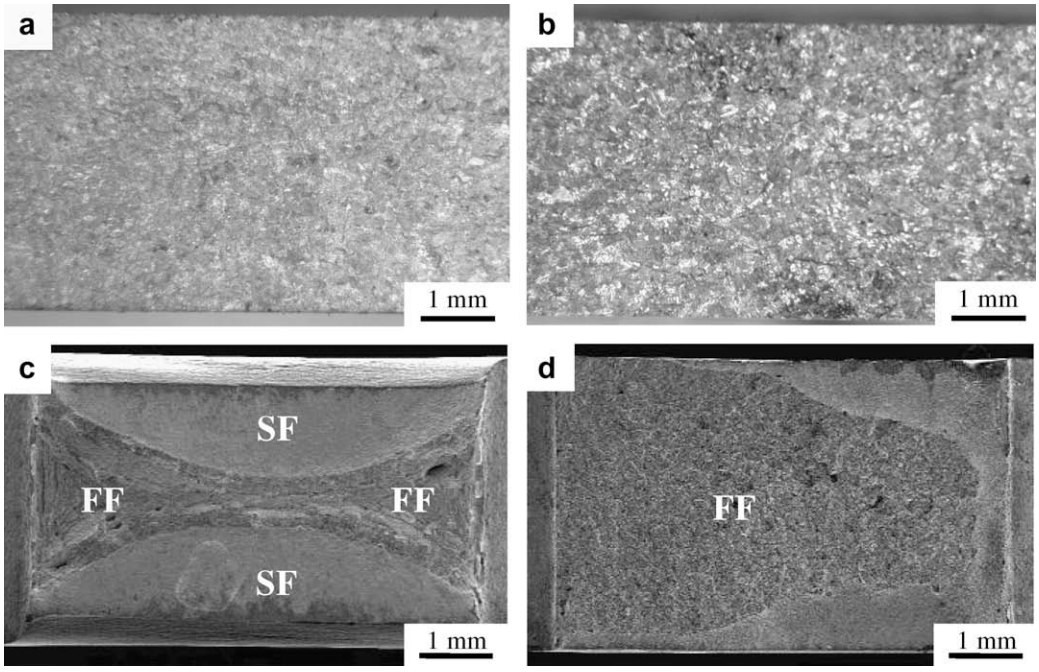

Fig. 5. Macro-fracture appearance of (a) the H1100 fatigue specimen in air, (b) the H1100 fatigue specimen in H_2, (c) the H1100 notched tensile specimen in H_2 and (d) the H800 notched tensile specimen in H_2.

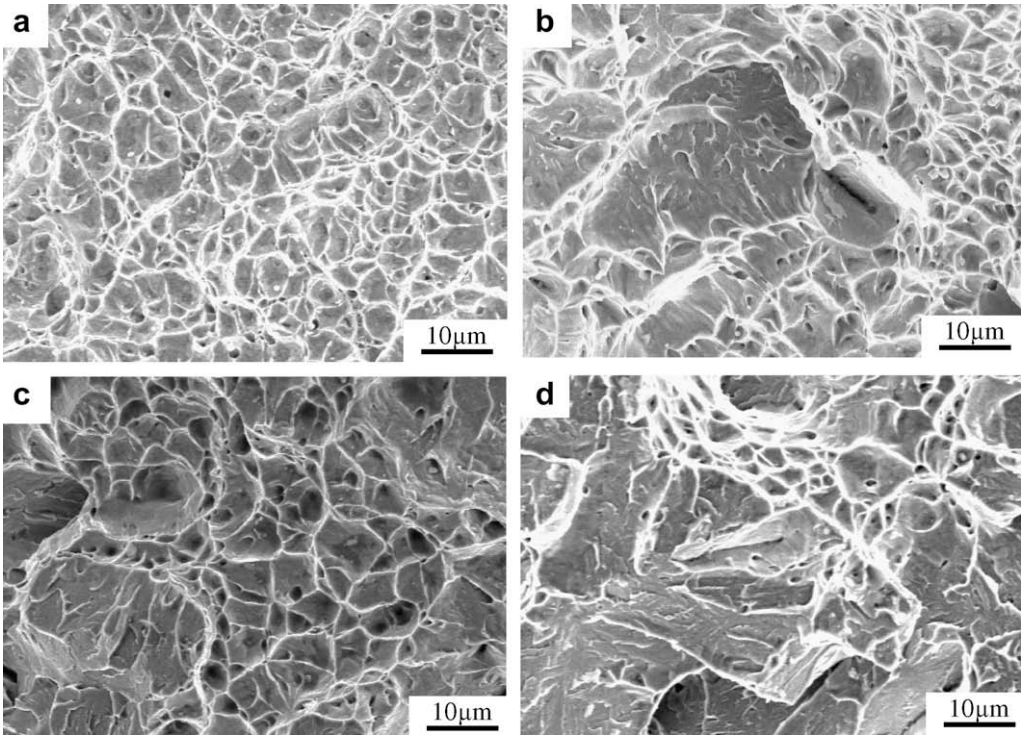

Fig. 6. SEM fractographs of: (a) the H1000 specimen, showing ductile dimple fracture after smooth tensile testing in air; (b) the H900 specimen, revealing a small amount of quasi-cleavage fracture mixed with dimple fracture after smooth tensile testing in air; (c) the H800 specimen, showing mixed mode fracture after notched tensile testing in H_2; and (d) the H900 specimen, revealing a greater extent of quasi-cleavage fracture after notched tensile testing in H_2.

stresses [24–26]. Hydrogen transport to the strained region is assisted predominantly by mobile dislocations [27]. High hydrogen concentrations in the high strained region lead to cracking therein. Additionally, high strength steel is generally associated with a small plastic zone ahead of the crack tip; hence, a critical hydrogen concentration can be reached promptly and can induce cracking thereafter. The low hydrogen diffusivity of the specimens aged at or above 593 °C, in addition to their reduced strength level, implies that a high concentration of hydrogen is less likely to be attained in the plastic zone in front of the crack tip, resulting in a decreased sulfide stress cracking susceptibility (or HE) of the material [10,20].

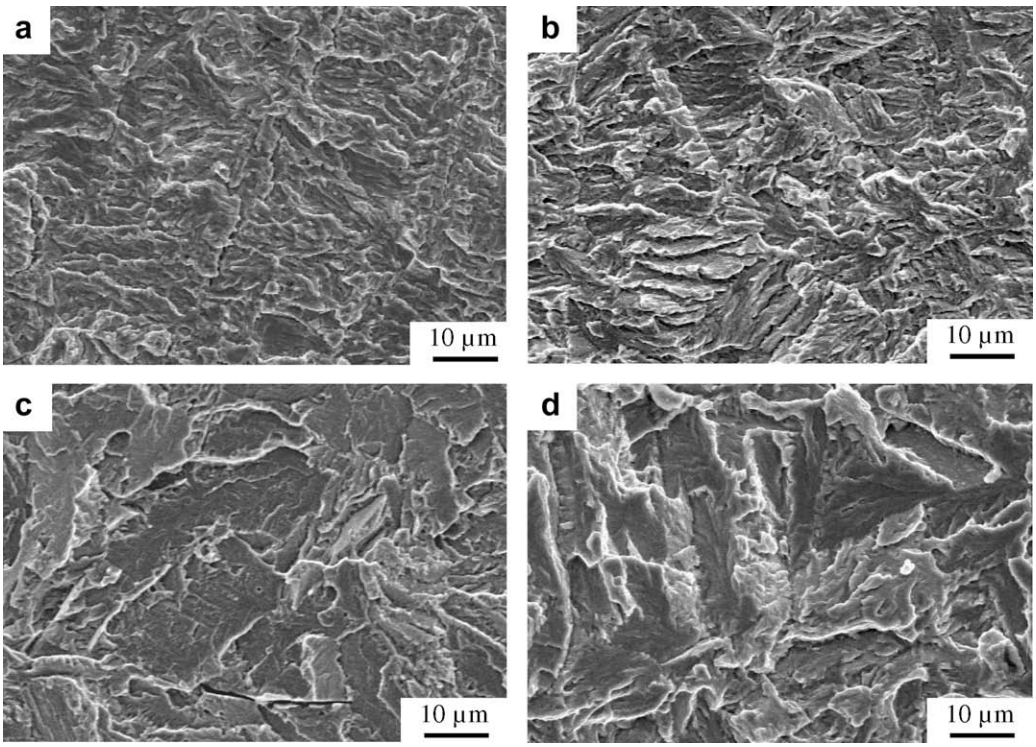

Fig. 7. SEM fatigue fractographs showing (a) the transgranular fatigue fracture of the ST specimen in air, (b) the transgranular fatigue, showing the trace of lath martensite morphology, for the H1200 specimen in air, (c) the extensive quasi-cleavage fracture of the H900 specimen in H_2, and (d) the reduced quasi-cleavage fracture of the H1200 specimen in H_2.

In this work, the trend of the hydrogen-accelerated fatigue crack growth of aged PH 13-8 Mo specimens was consistent with the susceptibilities to gaseous HE evaluated by slow extension rate tensile tests. The specimens with high NTS losses in hydrogen generally displayed rapid FCGRs. It was deduced that the same fracture mechanism was operating in these two types of specimens, regardless of loading conditions. Generally, higher strengths resulted in higher FCGRs and NTS losses of the material. The H800 and H900 specimens exhibit rapid FCGRs and high NTS losses in hydrogen, which could be attributed to their high strength levels associated with a high hydrogen concentration in the small plastic zone ahead of the crack tip. Therefore, the strength level played a very important role in affecting the HE susceptibility of the material. Furthermore, the difference in hydrogen-assisted cracking between specimens at the same yield strength level was notable, as illustrated with the H800 and H1100 specimens or the ST and H1200 specimens. This was also related to the microstructures of the different specimens. For instance, an increased amount of reverted austenite and relatively coarse precipitates in the over-aged specimens are known to decrease the hydrogen diffusivity and the HE susceptibility under static loading [10]. The retardation of hydrogen diffusion into the strained region, due to the presence of beneficial strong traps such as austenite, could effectively reduce the HE susceptibility of the alloy. This could also be extended to the situation of hydrogen-accelerated fatigue crack growth of the CT specimens. Besides, the existence of ductile austenite is beneficial to the toughness of the material [4,5], thereby reduce the FCGR of the over-aged specimens.

Structural steels are usually used in an over-aged condition with a reduced strength in order to overcome the influence of HE [28]. In general, high strength alloy steels in over-aged conditions are more resistant to sulfide stress corrosion cracking and hydrogen embrittlement [17,21,22]. This seems to be applicable to the PH 13-8 Mo steel. At the same strength level, over-aged (H1100 and H1200) specimens were more resistant to hydrogen-assisted fatigue crack growth than under-aged (H800) or un-aged (ST) specimens. The same tendency has been observed with AISI 630 precipitation-hardening stainless steel (17-4 PH). Fig. 8 displays the results of FCGR vs. ΔK for AISI 630 specimens, in which the H1150 (620 °C/4 h) specimen reveals a lower FCGR in hydrogen than the solution-treated (ST) specimen. Note that the solution-treated AISI 630 specimen had an ultimate tensile strength of 1135 MPa and a yield strength of 1009 MPa. For the same alloy in the over-aged condition, e.g., the H1150 specimen, the ultimate tensile and yield strengths were 1070 MPa and 990 MPa, respectively.

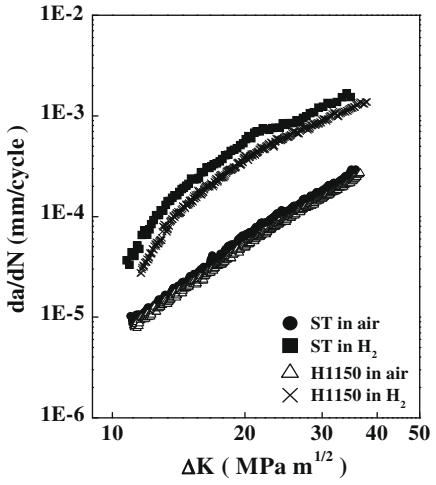

Fig. 8. Fatigue crack growth behaviors of AISI 630 specimens tested in air and hydrogen.

5. Conclusions

1. Hydrogen-accelerated FCGRs and reduced NTSs were found at various degrees for the aged PH 13-8 Mo specimens. In general, higher FCGRs for the specimen in hydrogen were consistent with the greater NTS losses. The specimens aged at 426 and 482 °C, with high strength levels, were affected the most by HE. The influence of HE became less for specimens aged at or above 593 °C.
2. For specimens at the same yield strength level, the over-aged specimens had better resistance to fatigue crack growth than the under-aged or un-aged specimens, despite of the testing environments. The presence of ductile reverted austenite in the over-aged specimens not only improved the toughness but also acted as beneficial traps for hydrogen, resulting in a reduced trend of hydrogen-accelerated crack growth and HE susceptibility.
3. The fatigue fracture appearance of all specimens revealed transgranular fatigue fracture in air, whereas extensive quasi-cleavage was seen for the specimens in hydrogen. A similar fracture mode was found for the fatigued specimens as the notched tensile specimens with high NTS losses in hydrogen. It was proposed that the same fracture mechanism could be applied to these two different types of specimens, regardless of loading conditions.
4. Slow extension rate tensile tests of sharp notch specimens could be considered as an alternative to evaluate qualitatively the accelerated crack growth of fatigue specimens in gaseous hydrogen or other more aggressive environments. If HE is a major concern in practical applications, a proper heat treatment to form beneficial hydrogen traps and tough microstructures should be considered. This is also an important consideration of high strength alloys in hydrogen storage applications.

References

[1] D.H. Ping, M. Ohnuma, Y. Hirakawa, Y. Kadoya, K. Hono, Mater. Sci. Eng. A 394 (2005) 285.
[2] V. Seetharaman, M. Sundararaman, R. Krishnan, Mater. Sci. Eng. 47 (1981) 1.
[3] L.W. Tsay, H.H. Chen, M.F. Chiang, C. Chen, Corr. Sci. 49 (2007) 2461.
[4] P.W. Hochandel, C.V. Robino, G.R. Edwards, M.J. Cieslak, Metall. Trans. 25A (1994) 789.
[5] P.D. Bilmes, M. Solari, C.L. Llorente, Mats. Charact. 46 (2001) 285.
[6] G.T. Murry, H.H. Honegger, T. Mousel, Corrosion 40 (1984) 146.
[7] P. Munn, B. Andersson, Corrosion 46 (1990) 286.
[8] J.R. Scully, M.J. Cieslak, J.A. Van Den Avyle, Scr. Metall. 31 (1994) 125.
[9] J.R. Scully, J.A. Van Den Avyle, M.J. Cieslak, A.D. Romig Jr., C.R. Hills, Metall. Trans. 22A (1991) 2429.
[10] L.W. Tsay, M.Y. Chi, H.R. Chen, C. Chen, Mater. Sci. Eng. A 416 (2006) 155.
[11] B.J. Berkowitz, F.H. Heubaum, Corrosion 44 (1984) 240.
[12] R. Gee, Z.Y. Chen, Corr. Sci. 37 (1995) 2003.
[13] L.W. Tsay, H.L. Lu, C. Chen, Corr. Sci. 50 (2008) 2506.
[14] R.R. Gaugh, Mater. Perf. 16 (1977) 24.
[15] J.A. Beavers, G.H. Koch, Corrosion 48 (1992) 256.
[16] A. Saxena, S.J. Hudak, Int. J. Fract. 14 (1978) 453.
[17] L.W. Tsay, C. Chen, S.L.I. Chan, Int. J. Mater. Product Tech. 10 (1995) 132.
[18] J. Xu, X.Z. Yuan, X.K. Sun, B.M. Wei, Scr. Metall. 29 (1993) 925.
[19] C. Gesnouin, A. Hazarabedian, P. Bruzzoni, J. Ovejero-García, P. Bilmes, C. Llorente, Corr. Sci. 46 (2004) 1633.
[20] L.W. Tsay, M.Y. Chi, J.K. Wu, D.L. Lin, Corr. Sci. 48 (2006) 1926.
[21] L.W. Tsay, W.C. Lee, R.K. Shiue*, J.K. Wu, Corr. Sci. 44 (2002) 2101.
[22] L.W. Tsay, W.C. Lee, W.C. Luu, J.K. Wu, Corr. Sci. 44 (2002) 1311.
[23] L.W. Tsay, W.B. Huang, C. Chen, Fat. Fract. Eng. Mat. Struct. 20 (1997) 1033.
[24] A.T. Yokobori Jr., T. Nemoto, K. Satoh, T. Yamada, Eng. Fract. Mech. 55 (1996) 47.
[25] J. Toribio, J. Mater. Sci. 28 (1993) 2289.
[26] J. Toribio, A.M. Lancha, M. Elices, Mater. Sci. Eng. A145 (1991) 167.
[27] A.M. Brass, J. Chêne, Corr. Sci. 48 (2006) 481.
[28] R.M. Thompson, G.B. Kohut, D.R. Canfield, W.R. Bass, Corrosion 47 (1991) 216.